

# PCCP

Accepted Manuscript



This is an *Accepted Manuscript*, which has been through the Royal Society of Chemistry peer review process and has been accepted for publication.

*Accepted Manuscripts* are published online shortly after acceptance, before technical editing, formatting and proof reading. Using this free service, authors can make their results available to the community, in citable form, before we publish the edited article. We will replace this *Accepted Manuscript* with the edited and formatted *Advance Article* as soon as it is available.

You can find more information about *Accepted Manuscripts* in the [Information for Authors](#).

Please note that technical editing may introduce minor changes to the text and/or graphics, which may alter content. The journal's standard [Terms & Conditions](#) and the [Ethical guidelines](#) still apply. In no event shall the Royal Society of Chemistry be held responsible for any errors or omissions in this *Accepted Manuscript* or any consequences arising from the use of any information it contains.

**A Comprehensive Study on Micellization of Dissymmetric Pyrrolidinium Headgroups Based  
Gemini Surfactants**

Min Zou<sup>1</sup>, Jinfeng Dong<sup>1</sup>, Guangfu Yang<sup>2</sup>, Xuefeng Li<sup>1,\*</sup>

1. College of Chemistry and Molecular Science, Wuhan University, Wuhan 430072, P.R. China.
2. Key Laboratory of Pesticide & Chemical Biology, Central China Normal University, Ministry of Education, Wuhan, 430079, P.R. China.

\*corresponding author, Email: [lixuefeng@whu.edu.cn](mailto:lixuefeng@whu.edu.cn)

**Abstract:**

Three groups of pyrrolidinium headgroups based Gemini surfactants 1, 1'-(propane-1, 3-diyl) bis (1-alkyl pyrrolidinium) bromide, in categories of the symmetric  $C_mC_3C_mPB$  ( $m = 10, 12, 14$ ), the dissymmetric  $C_mC_3C_{14}PB$  ( $m = 10, 12, 14$ ) and  $C_mC_3C_nPB$  ( $m = 8, 10, 12, m + n = 24$ ), are studied by equilibrium surface tension, conductivity, fluorescence, and NMR techniques. The importance of the dissymmetry on the micellization has been revealed in detail. The increase in the hydrophobic chain length  $m$  for  $C_mC_3C_mPB$  and  $C_mC_3C_{14}PB$  or in the dissymmetry ( $n/m$ ) for  $C_mC_3C_nPB$  can strengthen the aggregation ability and surface activity of surfactants significantly, *i.e.*, the lower critical micelle concentration ( $cmc$ ) and the lower surface tension at  $cmc$  ( $\gamma_{cmc}$ ). However, the aggregation number at  $cmc$  ( $N^*$ ) obeys the opposite variation tendency that it becomes smaller upon increasing  $m$  or  $n/m$  due to the formation of premicelles. Thermodynamic results reveal that the contribution of enthalpy ( $\Delta H_m^0$ ) to Gibbs free energy ( $\Delta G_m^0$ ) is strengthened by increasing  $m$  or  $n/m$  during the spontaneous micellization process. Moreover,  $^1H$  NMR results confirm the microenvironment changes of surfactants from polar water circumstance into micelles during the micellization, and 2D Noesy NMR spectra suggest that the location of methylene groups in the ring should adopt a confirmation toward the nonpolar micellar core rather than in the polar water circumstance.

**Keywords:**

Dissymmetric Gemini surfactant; surface tension; critical micelle concentration; aggregation number; thermodynamics of micellization

## 1. Introduction

Interests on surfactants, especially in developing those with new structures and functions [1~3], fabricating novel self-organized assemblies [4~6], and revealing their interactions on the molecular level [7, 8], have grown in the past decades. Undoubtedly, Gemini surfactants, the "dimers" of single-tailed surfactants covalently connected by a spacer group [9, 10], are one of the most attractive categories. Gemini surfactant shows overwhelming superiority in physicochemical properties according to its monomeric type, such as remarkably low critical micelle concentration (*cmc*) and high surface activity [9~11]. As results, they exhibit better foaming, wetting and solubilization capabilities, and therefore are applied widely in the fields of drug delivery, nano-material, and functional materials preparation *etc.* [12~15]

The *m-s-m* type Gemini surfactants (alkanediyl- $\alpha, \omega$ -bis (dimethyl-alkylammonium bromide)) are the most studied, both the hydrophobic chain length and the spacer length of them affect the physicochemical properties much [16~20]. The chemical incorporation of heterocycle headgroups, such as pyrrolidinium, hexahydropyridine and imidazolium groups, have significant effects on the physicochemical properties of surfactants [21~25]. Compared with the symmetric *m-s-m* type Gemini surfactants, those having the dissymmetric hydrophobic chain (*n-s-m*) show ever higher surface activity and lower *cmc* [26~29], which have advantages for applications in the life sciences. For example, Wettig *et.al.* found out that there are distinct differences between the interaction of symmetric *vs.* dissymmetric Gemini surfactant with DNA, and the latter one was more efficient as transfection reagents [30, 31]. Thus, the introduction of dissymmetry in Gemini surfactants sheds new light on the possibility of adjusting the adsorption and aggregation behaviors further.

We have recently reported a series of pyrrolidinium headgroups based Gemini surfactants, 1, 1'-(alkane-1, *s*-diyl) bis (1-alkyl pyrrolidinium) bromide ( $C_mC_sC_mPB$ ) [32, 33]. The effects of the hydrophobic chain length  $m$  and the spacer length  $s$  have been studied in detail, and our previous studies suggest that  $C_mC_sC_mPB$  may have better surface activity and aggregation ability than that of  $m$ - $s$ - $m$ . However, the influence of the dissymmetry is still unknown. The motivation of this work is to clarify the importance of dissymmetry on those surfactants, and to establish the structure-property relationships of them. Herein, we have synthesized several dissymmetric Gemini surfactants of 1, 1'-(propane-1, 3-diyl) bis (1-alkyl pyrrolidinium) bromide (Supporting Information Scheme S1), and the corresponding structures are shown in Scheme 1.

(Scheme 1)

Those surfactants can be divided into three groups, in categories of the symmetric  $C_mC_3C_mPB$  ( $m = 10, 12, 14$ ), the dissymmetric  $C_mC_3C_{14}PB$  ( $m = 10, 12, 14$ ) with those having 14 carbon atoms in one hydrophobic chain, and the dissymmetric  $C_mC_3C_nPB$  ( $m = 8, 10, 12, m + n = 24$ ) with those having the same carbon number of 24 totally in the two hydrocarbon chains. Thus, we can comparatively study the influence of hydrophobic chain dissymmetry on the micellization behaviors systematically. In this work, micellization properties such as *cmc*, the aggregation number, and thermodynamic parameters are obtained by employing equilibrium surface tension, conductivity and fluorescence measurements. Furthermore, the microenvironment changes of surfactants during the micellization and the confirmation of surfactants in micelles are studied by NMR techniques. The structure-property relationships of those surfactants are illustrated on the molecular level well.

## 2. Materials and methods

### 2.1 Materials

The pyrrolidinium headgroups based Gemini surfactants are synthesized according to the procedure mentioned in the Supporting Information Scheme S1. Pyrene (98 %) is purchased from Acros and recrystallized from ethanol. Benzophenone (99 %) and D<sub>2</sub>O (99.8 atom % D) are purchased from Acros and used as received. Ultrapure deionized water of Milli-Q grade is used in all experiments.

### 2.2 Equilibrium surface tension measurements

The equilibrium surface tension is conducted on K100 (Krüss, Germany) by employing the Du Noüy ring method. All measurements are performed at 25.0 ± 0.1 °C and repeated at least twice.

The adsorption amount at the air/water interface is obtained based on the Gibbs adsorption equation (1):

$$\Gamma_{\max} = -\frac{1}{2.303nRT} \cdot \frac{d\gamma}{d \log_{10} c} \quad (1)$$

where  $\Gamma_{\max}$  is the saturated adsorption amount in  $\mu\text{mol} \cdot \text{m}^{-2}$ ,  $\gamma$  is the surface tension in  $\text{mN} \cdot \text{m}^{-1}$ ,  $R$  is the gas constant,  $T$  is the absolute temperature, and  $c$  is the surfactant concentration. The value of prefactor  $n$  is dependent on the specific circumstances, and 3 is used according to the literatures [9, 17].

The minimum average occupied area per molecule ( $A_{\min}$ ) is obtained from the saturated adsorption using equation (2):

$$A_{\min} = \frac{1}{N_A \Gamma_{\max}} \times 10^{24} \quad (2)$$

where  $N_A$  is the Avogadro constant and  $A_{\min}$  is in  $\text{nm}^2$ .

### 2.3 Conductivity measurements

The conductivity is measured as a function of surfactant concentration with a low-frequency conductivity analyzer (DDSJ-308A, Shanghai Precision & Scientific Instrument Co. Ltd., accuracy of  $\pm 1\%$ ) at five different temperatures. The measurement is repeated three times at each temperature. Temperature is controlled at  $T \pm 0.1\text{ }^\circ\text{C}$  by using a HAAKE DC 30 thermostatic bath (Karlsruhe, Germany). The phase separation model is applied to obtain the thermodynamic parameters of micellization. The standard Gibbs free energy change of micellization is calculated from the following equation (3) [32, 33]:

$$\Delta G_m^0 = RT(0.5 + \beta) \ln(x_{cmc}) \quad (3)$$

where  $x_{cmc}$  is the *cmc* in molar fraction,  $\beta$  is the degree of counter ion binding to micelles,  $R$  is the gas constant,  $T$  is the absolute temperature. The standard enthalpy change for the micellization process,  $\Delta H_m^0$ , is determined by using the Gibbs–Helmholtz equation:

$$\Delta H_m^0 = \left[ \frac{\partial(\Delta G_m^0 / T)}{\partial(1/T)} \right] \quad (4)$$

$$\Delta H_m^0 = -RT^2(0.5 + \beta) d \ln(x_{cmc}) / dT \quad (5)$$

The standard entropy of micelle formation,  $\Delta S_m^0$ , is calculated according to the following relation:

$$\Delta S_m^0 = (\Delta H_m^0 - \Delta G_m^0) / T \quad (6)$$

### 2.4 Steady-state fluorescence quenching measurements

Steady-state fluorescence quenching (SSFQ) measurements are carried out on a RF-5301 PC fluorescence spectrophotometer using 1.0 cm quartz cell. Pyrene is used as a fluorescence probe with a constant concentration of  $1 \times 10^{-6}$  mol/L, and benzophenone is used as a quencher of the fluorescence probe. Pyrene spectra are recorded with fixed excitation at 335 nm, and the emission

spectra is scanned over the spectral range of 350-480 nm, the slit widths of excitation and emission are fixed at 5 nm and 1.5 nm, respectively.

For mono-dispersed micelles, the intensities ( $I$ ) and the aggregation number ( $N_{agg}$ ) fit to the following equation (7) [34]:

$$\ln\left(\frac{I_0}{I}\right) = \frac{N_{agg}c_Q}{c_s - cmc} \quad (7)$$

where  $I_0$  and  $I$  are the fluorescence intensities of pyrene probe with and without quencher, respectively.  $c_Q$  and  $c_s$  are the concentration of quencher and surfactant, respectively.

## 2.5 NMR measurements

All NMR measurements are performed on a 400 MHz Bruker-BioSpin spectrometer at 25 °C. 2D Noesy spectra are performed with the standard pulse sequences. A 90° pulse width of 8.2  $\mu$ s, a mixing time of 100, 300 or 500  $ms$ , a relaxation delay of 2  $s$ , and an acquisition time of 205  $ms$  are used. The experimental data are collected 2048 complex points, and processed with a Lorentz-to-Gauss window function and zero filling in both dimensions to display data on a 2048  $\times$  2048 2D-matrix. The peaks are referenced with respect to DOH ( $\delta = 4.790$  ppm) in D<sub>2</sub>O.

## 3 Results and Discussion

### 3.1 Equilibrium surface adsorption behaviors

The equilibrium surface adsorption behaviors of Gemini surfactants, including C<sub>10</sub>C<sub>3</sub>C<sub>10</sub>PB, C<sub>12</sub>C<sub>3</sub>C<sub>12</sub>PB, C<sub>14</sub>C<sub>3</sub>C<sub>14</sub>PB, C<sub>12</sub>C<sub>3</sub>C<sub>14</sub>PB, C<sub>10</sub>C<sub>3</sub>C<sub>14</sub>PB and C<sub>8</sub>C<sub>3</sub>C<sub>16</sub>PB, are evaluated by the surface tensionmetry using the du Noüy ring method, and the equilibrium surface tension as a function of surfactant concentration is obtained (Figure 1). The clear breakpoints in the  $\gamma - \log_{10} c$  curve indicate the onset of micellization, and the absence of a minimum around the breakpoints confirms

the purity of the surfactants.

(Figure 1)

The adsorption efficiency of surfactant at the air/water surface is often determined by  $pC_{20}$  ( $pC_{20} = -\log_{10} c_{20}$ ), which is the surfactant concentration ( $c_{20}$ ) required for lowering the surface tension of water by  $20 \text{ mN}\cdot\text{m}^{-1}$  [32]. Generally, the larger the  $pC_{20}$ , the higher adsorption efficiency of the surfactant is. Based on the  $\gamma - \log_{10} c$  curves, some important physicochemical parameters of them such as  $cmc$ ,  $\gamma_{cmc}$ ,  $A_{\min}$  and  $pC_{20}$  are extracted and listed in Table 1.

(Table 1)

Figure 2a shows that the  $cmc$  values of both the symmetric  $C_mC_3C_mPB$  and the dissymmetric  $C_mC_3C_{14}PB$  series decrease linearly with the increase of the total carbon number ( $N_c$ ) in the hydrocarbon chains, resulting in two linear equations of  $\log_{10} cmc = 1.14 - 0.182 \times N_c$  and  $\log_{10} cmc = -1.86 - 0.0738 \times N_c$  for  $C_mC_3C_mPB$  and  $C_mC_3C_{14}PB$ , respectively. Obviously, both the symmetric  $C_mC_3C_mPB$  and the dissymmetric  $C_mC_3C_{14}PB$  series follow the well-known Klevens empirical equation of  $\log_{10} cmc = A - B \times N_c$  well, where  $A$  and  $B$  are empirical constants [35]. The two values of  $B$ , reflecting the contribution of each additional methylene unit on the  $cmc$ , are significantly different. The difference in  $B$  values indicates that the increase in the hydrophobic chain length for the symmetric Gemini surfactant is more efficient in enhancing aggregation ability than that of the dissymmetric one. Though the  $cmc$  values of the dissymmetric  $C_mC_3C_{14}PB$  are far smaller than those of the symmetric  $C_mC_3C_mPB$ , however, the contribution of each additional methylene unit to  $C_mC_3C_{14}PB$  is more like that of the classic single-tailed surfactant homologues [32]. It is noticed that  $\gamma_{cmc}$  of either  $C_mC_3C_mPB$  or  $C_mC_3C_{14}PB$  decreases with the increase of  $N_c$  regardless of the dissymmetry (Supporting Information Figure S1a), indicating the

longer hydrophobic chain length, the higher the surface activity is, which can also be observed from pC<sub>20</sub>. However,  $A_{\min}$  of C<sub>m</sub>C<sub>3</sub>C<sub>m</sub>PB and C<sub>m</sub>C<sub>3</sub>C<sub>14</sub>PB increases with the increase of  $N_c$  because the longer hydrophobic chains are more prone to bend [32].

(Figure 2)

The typical effect of the dissymmetry on *cmc* can be clearly observed from C<sub>m</sub>C<sub>3</sub>C<sub>n</sub>PB series (Figure 2b), those having the same carbon number of 24 in the hydrocarbon chains. It is clear that the higher dissymmetry results in the lower *cmc* by employing the  $n/m$  as the degree of dissymmetry. The *cmc* values follow a linear relationship of  $\log_{10} cmc = -1.88 - 1.305 \times n/m$ , and similar linear relationship is also observed from other dissymmetric ones [27]. This observation indicates that the introduction of dissymmetry in the hydrophobic chains can strengthen the aggregation ability. At the same time, the increase in the dissymmetry ( $n/m$ ) results in the decrease of  $\gamma_{cmc}$  and  $A_{\min}$  of C<sub>m</sub>C<sub>3</sub>C<sub>n</sub>PB (Supporting Information Figure S1b). The decrease in  $A_{\min}$  suggests that surfactants with the higher dissymmetry are packed closer at the air/water surface, and therefore result in a lower  $\gamma_{cmc}$ .

### 3.2 Micellar aggregation number

The micellar aggregation number ( $N_{\text{agg}}$ ) is measured by the SSFQ method, and the concentration dependent  $N_{\text{agg}}$  of C<sub>10</sub>C<sub>3</sub>C<sub>10</sub>PB, C<sub>12</sub>C<sub>3</sub>C<sub>12</sub>PB, C<sub>14</sub>C<sub>3</sub>C<sub>14</sub>PB, C<sub>12</sub>C<sub>3</sub>C<sub>14</sub>PB, C<sub>10</sub>C<sub>3</sub>C<sub>14</sub>PB and C<sub>8</sub>C<sub>3</sub>C<sub>16</sub>PB is shown in Figure 3. Since the employed concentration ( $c$ ) is changed from about 0.1 to 100 mmol/L due to the significant difference in their *cmc* values, and therefore  $c/cm_c$  is used to evaluate the concentration dependence instead of  $c$ . Figure 3 shows that  $N_{\text{agg}}$  is increased nearly linearly with  $c/cm_c$  in the measured concentration region for each surfactant. The increase in  $N_{\text{agg}}$  upon increasing surfactant concentration indicates the micellar growth. This is because the

electrostatic repulsion among surfactants are reduced when the surfactant concentration is increased, which favors the micellar growth [33].

(Figure 3)

In order to clarify the importance of the hydrophobic chain length ( $m$ ) and the dissymmetry ( $n/m$ ) on the micellar aggregation number, the micellar aggregation number at  $cmc$  ( $N^*$ ) is employed rather than  $N_{agg}$  to avoid the effect of concentration variation, which is derived from Figure 3 and listed in Table 1. The  $N^*$  values of  $C_{10}C_3C_{10}PB$ ,  $C_{12}C_3C_{12}PB$  and  $C_{14}C_3C_{14}PB$  are 13, 12 and 5, respectively, indicating  $N^*$  is decreased with the increase of the hydrophobic length for the symmetric  $C_mC_3C_mPB$  series (Figure 4a). Those of  $C_{10}C_3C_{14}PB$ ,  $C_{12}C_3C_{14}PB$  and  $C_{14}C_3C_{14}PB$  are 8, 6 and 5, respectively, suggesting the changes of  $N^*$  of the dissymmetric  $C_mC_3C_nPB$  follows the same tendency as that of  $C_mC_3C_mPB$ . For the  $C_mC_3C_nPB$  series, those having the same carbon number of 24 totally in the two hydrocarbon chains, the decrease in  $N^*$  is also observed when  $n/m$  is increased (Figure 4b).

(Figure 4)

The changes in  $N^*$  reveal that the increase in  $m$  or  $n/m$  is not beneficial to larger micelles formation, which is significantly different from what happens in its corresponding monomeric one [36]. The aggregation ability of surfactant is often enhanced upon increasing the hydrophobic chain length because the hydrophobic force is strengthened, and therefore results in a larger aggregation number [37, 38]. Similar decrease in  $N_{agg}$  was also observed in other Gemini surfactant homologies, such as in the imidazolium type Gemini surfactants ( $[C_m-3-C_mim]Br_2$ ) [39] and the nitrophenoxy groups containing Gemini surfactants ( $Nm-6-mN$ ) [40]. Previous studies on Gemini surfactants show that Gemini surfactants can form premicelles in the aqueous solution,

and the tendency will be strengthened upon increasing the hydrophobic chain length or the spacer length [9, 33, 37, 40]. Generally, the longer the hydrophobic chain length of surfactant is, the more premicelles be formed. Obviously, the high percentage of premicelles will result in the decrease of the average aggregation number for a given Gemini surfactant. Thus, the increase in both  $m$  and  $n/m$  induced  $N^*$  decrease should be attributed to the formation of premicelles. The more premicelles form, the lower  $N^*$  is. Herein, all the measured  $N^*$  values are below 13, especially that of  $C_8C_3C_{16}PB$  is only 2, which highly support the formation of premicelles [37].

### 3.3 Micellization thermodynamic parameters

To make a better understand on the influence of the dissymmetry on the micellization behaviors, the micellization thermodynamics is studied based on the temperature dependent electrical conductivity measurements (Supporting Information Figure S2). The corresponding micellization thermodynamic parameters at different temperature are listed in Table 2 and the  $cmc$  values at 25 °C are shown in Table 1. Clearly, all the  $cmc$  values measured by surface tension and conductivity methods for each surfactant are consistent very well.

(Table 2)

Generally speaking, the standard Gibbs free energy change ( $\Delta G_m^0$ ) is negative for each surfactant at the given temperature, showing the spontaneous micellization process. It is noticed that the hydrophobic chain length and the dissymmetry strongly affect  $\Delta G_m^0$ , or in other words, the micellization process (Figure 5).  $\Delta G_m^0$  is increased when the hydrophobic chain length is increased for both the symmetric  $C_mC_3C_mPB$  and the dissymmetric  $C_mC_3C_{14}PB$  series (Figure 5a), indicating the longer hydrocarbon chain favors micellization due to the greater hydrophobic interactions. However, the higher degree of dissymmetry ( $n/m$ ) results in the lower  $|\Delta G_m^0|$  as has

been observed from the  $C_mC_3C_nPB$  series, suggesting the higher degree of dissymmetry is not beneficial to the micellization (Figure 5b). The result is distinguished from that of  $n-6-m$  type Gemini surfactants [27], in which  $|\Delta G_m^0|$  only increases slightly with the increase of the dissymmetry.

(Figure 5)

According to the thermodynamic models of micellization [41],  $\Delta G_m^0$  reflects the total contribution of surfactants in micelles, which is highly related to the micellar size or the micellar aggregation number. Since the high degree of dissymmetry favors premicelles formation as mentioned in section 3.2, thus the dissymmetry induced  $|\Delta G_m^0|$  decrease (Figure 5b) can also be attributed to the formation of premicelles. In other words, the more premicelles form, the smaller  $|\Delta G_m^0|$  is. Recalling to the dissymmetry induced aggregation ability increase in section 3.1, the effect of the dissymmetry on micellization is clear that the dissymmetry in the hydrophobic chains favors micellization strongly, whereas only those with a smaller aggregation number or premicelles will be formed.

Simultaneously, the standard enthalpy changes ( $\Delta H_m^0$ ) is also negative for each surfactant, indicating the micellization process is an exothermic process. Moreover, the value of  $|-T \cdot \Delta S_m^0|$  is often larger than that of  $|\Delta H_m^0|$  at a given temperature, *i.e.* at 25 °C, indicating an entropy-driven process. However, the hydrophobic chain length and the dissymmetry affect the contribution of  $\Delta H_m^0$  to  $\Delta G_m^0$  strongly. Figure 6 shows that the contribution of  $\Delta H_m^0$  is increased when the hydrophobic chain length  $m$  is increased for both the symmetric  $C_mC_3C_mPB$  and the dissymmetric  $C_mC_3C_{14}PB$ . Our previous study on  $C_mC_4C_mPB$  shows that the micellization is an enthalpy-driven process rather than an entropy-driven process when  $m$  was above 14 [32], which supports the

results well. It is also noticed that the higher degree of dissymmetry ( $n/m$ ) results in the higher contribution of  $\Delta H_m^0$  for the  $C_mC_3C_nPB$  series, and the micellization of  $C_8C_3C_{16}PB$  is even enthalpy-driven instead of entropy-driven. Since similar phenomenon is also observed in other dissymmetric Gemini surfactants [26, 27], the introduction of the dissymmetry in the hydrophobic chain induced enthalpy-driven force strengthen might be universal for Gemini surfactants during the micellization.

(Figure 6)

### 3.4 NMR studies

Three Gemini surfactants of  $C_{10}C_3C_{10}PB$ ,  $C_{12}C_3C_{12}PB$  and  $C_{10}C_3C_{14}PB$  are study by NMR techniques. From the point of molecular structures, both the hydrophobic chain length and the dissymmetry are considered. Since the dissymmetry shows little effect on the  $^1H$  NMR spectra, therefore only those of  $C_{10}C_3C_{14}PB$  are typically shown (Figure 7), others are shown in the Supporting Information Figure S3.

(Figure 7)

Figure 7 shows that the chemical shifts of  $C_{10}C_3C_{14}PB$  change greatly upon increasing its concentrations. To make a better understand, the chemical shifts of three typical protons such as  $H_a$  and  $H_c$  in the headgroups and  $H_w$  in the hydrophobic tails for each surfactant are plotted versus surfactant concentrations (Supporting Information Figure S4). Clearly, the chemical shifts of  $H_a$ ,  $H_c$  and  $H_w$  remain nearly constant at low concentration, whereas shift toward downfield significantly when the surfactant concentration is above a special value, indicating the micellization. Micelle can be considered as a closed monolayer with the solvated hydrophilic headgroups of surfactants in micelle toward the water circumstance, and thus results in a nonpolar

oil-like or hydrophobic core [38]. Therefore, surfactant monomers will transfer from the polar water circumstance into micelles, the less polar microenvironment, during the micellization [42]. The decrease of polarity in solvation commonly leads to the downshift of  $^1\text{H}$  NMR signal for the protons in surfactant.

There presents a quantitative relationship between chemical shifts and concentration of surfactant as following [43]:

$$\delta_{\text{obs}} = \delta_{\text{mic}} - \left( \frac{cmc}{c_T} \right) (\delta_{\text{mic}} - \delta_{\text{mon}}) \quad (8)$$

where  $\delta_{\text{obs}}$ ,  $\delta_{\text{mon}}$  and  $\delta_{\text{mic}}$  represent the observed chemical shift of surfactant, the chemical shift of surfactant in its monomer and the micellar form, respectively.  $cmc$  and  $c_T$  are the critical micelle concentration and the total surfactant concentration. According to the equation (8), the plot of  $\delta_{\text{obs}}$  versus  $1/c_T$  should yield two straight lines with the intersection corresponding to the  $cmc$  [43, 44]. Based on the plots of  $\delta_{\text{obs}}$  versus  $1/c_T$  (Figure 8), the average  $cmc$  values of obtained from  $H_a$ ,  $H_c$  and  $H_w$  are  $3.34 \pm 0.03$ ,  $0.517 \pm 0.05$  and  $0.407 \pm 0.032$  mM for  $\text{C}_{10}\text{C}_3\text{C}_{10}\text{PB}$ ,  $\text{C}_{12}\text{C}_3\text{C}_{12}\text{PB}$  and  $\text{C}_{10}\text{C}_3\text{C}_{14}\text{PB}$ , respectively, which are consistent with those measured by surface tension and conductivity.

(Figure 8)

2D Noesy NMR spectra of  $\text{C}_{10}\text{C}_3\text{C}_{10}\text{PB}$ ,  $\text{C}_{12}\text{C}_3\text{C}_{12}\text{PB}$  and  $\text{C}_{10}\text{C}_3\text{C}_{14}\text{PB}$  show similar intermolecular interactions, indicating that surfactants should adopt similar confirmation in micelles regardless of the hydrophobic chain length and the dissymmetry. Typical 2D Noesy NMR spectrum of  $\text{C}_{12}\text{C}_3\text{C}_{12}\text{PB}$  is shown in Figure 9, and those of  $\text{C}_{10}\text{C}_3\text{C}_{10}\text{PB}$  and  $\text{C}_{10}\text{C}_3\text{C}_{14}\text{PB}$  are shown in the Supporting Information Figure S5. Clearly, there presents interactions between the headgroup protons and those in the middle of the hydrophobic chain, *i.e.* the interactions between

$H_a$  and  $H_c$  or  $H_b$  and  $H_c$ , except the strong interactions between  $H_a$  and  $H_b$ . The results strongly suggest that the location of methylene groups in the ring should be very close to the hydrophobic chain [45]. In other words, they should adopt a confirmation toward the nonpolar micellar core rather than in the polar water circumstance, and exhibit some hydrophobic contribution during micellization. Our previous study on  $C_mC_4C_m$ PB revealed that both the surface activity and micellization ability of  $C_mC_4C_m$ PB were much stronger than those of  $m-4-m$  type Gemini surfactants with the same hydrophobic chain length [32], which support the idea well.

(Figure 9)

#### 4. Conclusions

In summary, a comprehensive study has been conducted on three groups of pyrrolidinium headgroups based Gemini surfactants 1, 1'-(propane-1, 3-diyl) bis (1-alkyl pyrrolidinium) bromide, including the symmetric  $C_mC_3C_m$ PB, the dissymmetric  $C_mC_3C_{14}$ PB and  $C_mC_3C_n$ PB. Compared with our previous studies on the effects of hydrophobic chain length and spacer length on micellization, this work focuses on the importance of the dissymmetry. *cmc* values of the surfactants decrease linearly with the increase of the total carbon number ( $N_c$ ) in the hydrocarbon chain or the dissymmetry ( $n/m$ ). The aggregation number at *cmc* ( $N^*$ ) becomes smaller upon increasing either  $m$  or  $n/m$  due to the formation of premicelles. Though all the micellization are spontaneous processes, and the entropy-driven process is often dominated. However, the contribution of enthalpy ( $\Delta H_m^0$ ) to Gibbs free energy ( $\Delta G_m^0$ ) is strengthened upon increasing  $m$  or  $n/m$  that the micellization of  $C_8C_3C_{16}$ PB is even transferred into an enthalpy-driven process. More importantly, the dissymmetry increase results in the decrease of  $\Delta G_m^0$ , and the formation of

premicelles should be the major cause. NMR results confirm the microenvironment changes of surfactants from polar water circumstance into micelles during micellization, and suggest the location of methylene groups in the ring should adopt a confirmation toward the nonpolar micellar core rather than in the polar water circumstance.

### Acknowledgements

This work was supported by the National Natural Science Foundation of China (NSFC 20973129 and 21273165).

### References

- [1] S. Landsmann, C. L. Pueyo and S. Polarz, *J. Am. Chem. Soc.*, 2010, **132**, 5315.
- [2] K. L. Jia, Y. M. Cheng, X. Liu, X. F. Lin and J. F. Dong, *RSC Adv.*, 2015, **5**, 640.
- [3] J. H. Li, Y. F. Tang, Q. W. Wang, X. F. Li, L. F. Cun, X. M. Zhang, J. Zhu, L. C. Li and J. G. Deng, *J. Am. Chem. Soc.*, 2012, **134**, 18522.
- [4] L. X. Jiang, J. W. J. de Folter, J. B. Huang, A. P. Philipse, W. K. Kegel and A. V. Petukhov, *Angew. Chem. Int. Ed.*, 2013, **52**, 3364.
- [5] P. A. Rugar, L. Chabanne, M. A. Winnik and I. Manners<sup>1</sup>, *Science*, 2012, **337**, 559.
- [6] T. G. Barclay, K. Constantopoulos and J. Matison, *Chem. Rev.*, 2014, **114**, 10217.
- [7] K. T. Nguyen, T. D. Nguyen and A. V. Nguyen, *Langmuir*, 2014, **30**, 7047.
- [8] J. F. Chenac and J. C. Hao, *Phys. Chem. Chem. Phys.*, 2013, **15**, 5563.
- [9] R. Zana, *Adv. Colloid Interface Sci.*, 2002, **97**, 205.
- [10] V. D. Sharma and M.A. Ilies, *Med. Res. Rev.*, 2014, **34**, 1.

- [11] A. Rodríguez, M. M. Graciani, A. J. Moreno-Vargas and M. L. Moyá, *J. Phys. Chem. B*, 2008, **112**, 11942.
- [12] A. J. Kirby, P. Camilleri, J. B. F. N. Engberts, M. C. Feiters, R. J. M. Nolte, O. Soderman, M. Bergsma, P. C. Bell, M. L. Fielden, C. L. G. Rodríguez, P. Guédat, A. Kremer, C. McGregor, C. Perrin, G. Ronsin and M. C. P. van Eijk, *Angew. Chem. Int. Ed.*, 2003, **42**, 1448.
- [13] C. P. Song, D. Q. Wu, F. Zhang, P. Liu, Q. H. Lu and X.L. Feng, *Chem. Commun.*, 2012, **48**, 2119.
- [14] T. Jain, A. R. Tehrani-Bagha, H. Shekhar, R. Crawford, E. Johnson, K. Nørgaard, K. Holmberg, P. Erhart and K. Moth-Poulsen, *J. Mater. Chem. C*, 2014, **2**, 994.
- [15] V. D. Sharma, J. Lees, N. E. Hoffman, E. Brailoiu, M. Madesh, S. L. Wunder and M. A. Ilies, *Mol. Pharm.*, 2014, **11**, 545.
- [16] P. X. Li, C. C. Dong, R. K. Thomas, J. Penfold and Y. L. Wang, *Langmuir*, 2011, **27**, 2575.
- [17] E. Alami, G. Beinert, P. Marie and R. Zana, *Langmuir*, 1993, **9**, 1465.
- [18] R. Zana, *J. Colloid Interface Sci.*, 2002, **246**, 182.
- [19] S. De, V. K. Aswal, P. S. Goyal and S. Bhattacharya, *J. Phys. Chem.*, 1996, **100**, 11664.
- [20] L. M. Bergström and V. M. Garamus, *Langmuir*, 2012, **28**, 9311.
- [21] L. Zhou, X. Jiang, Y. Li, Z. Chen, X. Hu, *Langmuir*, 2007, **23**, 11404.
- [22] F. M. Menger, J. S. Keiper and V. Azov, *Langmuir*, 2000, **16**, 2062.
- [23] M. Ao, G. Xu, Y. Zhu, Y. Bai, *J. Colloid Interface Sci.*, 2008, **326**, 490.
- [24] Z. Jiang, X. F. Li, G. F. Yang, L. Cheng, B. Cai, Y. Yang and J. F. Dong, *Langmuir*, 2012, **28**, 7174.
- [25] J. L. Anderson, R. Ding, A. Ellern and D. W. Armstrong, *J. Am. Chem. Soc.*, 2005, **127**, 593.

- [26] G. Y. Bai, J. B. Wang, Y. J. Wang, H. K. Yan and R. K. Thomas, *J. Phys. Chem. B*, 2002, **106**, 6614.
- [27] X. Y. Wang, J. B. Wang, Y. L. Wang, J. P. Ye, H. K. Yan and R.K. Thomas, *J. Phys. Chem. B*, 2003, **107**, 11428.
- [28] M. Sikirić , I. Primožič , Y. Talmon and N. Filipović-Vinceković, *J. Colloid Interface Sci.*, 2005, **281**, 473.
- [29] R. Oda, I. Huc, J. C. Homo, B. Heinrich, M. Schmutz and S. Candau, *Langmuir*, 1999, **15**, 2384.
- [30] S. D. Wettig, R. Deubry, J. Akbar, T. Kaur, H. T. Wang, T. Sheinin, J. W. Joseph and R. A. Slavcev, *Phys. Chem. Chem. Phys.*, 2010, **12**, 4821.
- [31] H. T. Wang and S. D. Wettig, *Phys. Chem. Chem. Phys.*, 2011, **13**, 637.
- [32] B. Cai, X. F. Li, Y. Yang and J. F. Dong, *J. Colloid Interface Sci.*, 2012, **370**, 111.
- [33] B. Cai, J. F. Dong, L. Cheng, Z. Jiang, Y. Yang and X. F. Li, *Soft Matter*, 2013, **9**, 7637.
- [34] A. R. Tehrani-Bagha, J. Kärnbratt, J. E. Löfroth and K. Holmberg, *J. Colloid Interface Sci.*, 2012, **376**, 126.
- [35] H. B. Klevens, *J. Am. Oil Chem. Soc.*, 1953, **30**, 74.
- [36] M. W. Zhao and L.Q. Zheng, *Phys. Chem. Chem. Phys.*, 2011, **13**, 1332.
- [37] J. H. Mathias, M. J. Rosen and L. Davenport, *Langmuir*, 2001, **17**, 6148.
- [38] *Surfactants and Interfacial Phenomena*, M. J. Rosen, 2nd ed., John Wiley & Sons, New York, 1989.
- [39] C. C. Ren, F. Wang, Z. Q. Zhang, H. H. Nie, N. Li and M. Cui, *Colloid Surface A*, 2015, **467**, 1.

- [40] X. Huang, Y. C. Han and Y. L. Wang, *Acta Chim. Sinica*, 2013, **71**, 897.
- [41] T. A. Camesano and R. Nagarajan, *Colloid Surface A*, 2000, **167**, 165.
- [42] Y. Jiang, H. Chen, X. H. Cui, S. Z. Mao, M. L. Liu, P. Y. Luo and Y. R. Du, *Langmuir*, 2008, **24**, 3118.
- [43] X. Huang, Y. C. Han, Y. X. Wang, M. W. Cao and Y. L. Wang, *Colloid Surface A*, 2008, **325**, 26.
- [44] Y. Zhao, S. J. Gao, J. J. Wang and J. M. Tang, *J. Phys. Chem. B*, 2008, **112**, 2031.
- [45] X. Y. Yang, H. Chen, G. Z. Cheng, S. Z. Mao, M. L. Liu, P. Y. Luo and Y. R. Du, *Colloid Polym. Sci.*, 2008, **286**, 639.

## Captions

**Scheme 1.** Molecular structures of pyrrolidinium headgroups based Gemini surfactants.

**Table 1.** Surface properties of pyrrolidinium headgroups based Gemini surfactants.

**Table 2.** Thermodynamic parameters of micellization at different temperatures.

**Figure 1.**  $\gamma - \log_{10} c$  curves of Gemini surfactants in aqueous solutions at 25 °C.

**Figure 2.** Effects of hydrophobic chain length (*a*) and dissymmetry (*b*) on *cmc*.

**Figure 3.** Concentration dependent micellar aggregation number ( $N_{agg}$ ) at 25 °C, the *cmc* values adopted from surface tension measurements.

**Figure 4.** Effect of the hydrophobic chain length (*a*) and the dissymmetry (*b*) on  $N^*$  at 25 °C.

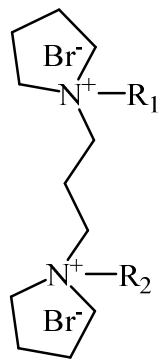
**Figure 5.** Effect of the hydrophobic chain length (*a*) and the dissymmetry (*b*) on  $\Delta G_m^0$  at 25 °C.

**Figure 6.** Contribution of enthalpy ( $\Delta H_m^0$ ) and entropy ( $-T \cdot \Delta S_m^0$ ) to Gibbs free energy ( $\Delta G_m^0$ ) at 25 °C.

**Figure 7.** Concentration dependent  $^1\text{H}$  NMR spectra and proton numbering of  $\text{C}_{10}\text{C}_3\text{C}_{14}\text{PB}$  in  $\text{D}_2\text{O}$  at 25 °C.

**Figure 8.** Plots of  $\delta_{obs}$  versus  $1/c_T$  for  $\text{C}_{10}\text{C}_3\text{C}_{10}\text{PB}$  (*a*),  $\text{C}_{12}\text{C}_3\text{C}_{12}\text{PB}$  (*b*) and  $\text{C}_{10}\text{C}_3\text{C}_{14}\text{PB}$  (*c*) at 25 °C in  $\text{D}_2\text{O}$ .

**Figure 9.** 2D Noesy NMR spectrum of 5 mM  $\text{C}_{12}\text{C}_3\text{C}_{12}\text{PB}$  in  $\text{D}_2\text{O}$  at 25 °C.



R <sub>1</sub>	R <sub>2</sub>	surfactants
C <sub>10</sub> H <sub>21</sub>	C <sub>10</sub> H <sub>21</sub>	C <sub>10</sub> C <sub>3</sub> C <sub>10</sub> PB
C <sub>12</sub> H <sub>25</sub>	C <sub>12</sub> H <sub>25</sub>	C <sub>12</sub> C <sub>3</sub> C <sub>12</sub> PB
C <sub>14</sub> H <sub>29</sub>	C <sub>14</sub> H <sub>29</sub>	C <sub>14</sub> C <sub>3</sub> C <sub>14</sub> PB
C <sub>12</sub> H <sub>25</sub>	C <sub>14</sub> H <sub>29</sub>	C <sub>12</sub> C <sub>3</sub> C <sub>14</sub> PB
C <sub>10</sub> H <sub>21</sub>	C <sub>14</sub> H <sub>29</sub>	C <sub>10</sub> C <sub>3</sub> C <sub>14</sub> PB
C <sub>8</sub> H <sub>17</sub>	C <sub>16</sub> H <sub>33</sub>	C <sub>8</sub> C <sub>3</sub> C <sub>16</sub> PB

**Scheme 1.** Molecular structures of pyrrolidinium headgroups based Gemini surfactants.

**Table 1.** Surface properties of pyrrolidinium headgroups based Gemini surfactants.

Surfactants	<i>cmc</i> (mol/L)		$\gamma_{cmc}$ (mN/m)	$\Gamma_{max}$ ( $\mu\text{mol}/\text{m}^2$ )	$A_{min}$ ( $\text{nm}^2$ )	pC <sub>20</sub>	$N^{*a}$
	Surface tension	Conductivity					
C <sub>10</sub> C <sub>3</sub> C <sub>10</sub> PB	$3.21 \times 10^{-3}$	$4.41 \times 10^{-3}$	37.6	1.42	1.17	3.11	13
C <sub>12</sub> C <sub>3</sub> C <sub>12</sub> PB	$6.02 \times 10^{-4}$	$6.68 \times 10^{-4}$	35.4	1.18	1.40	4.12	12
C <sub>14</sub> C <sub>3</sub> C <sub>14</sub> PB	$1.13 \times 10^{-4}$	$1.14 \times 10^{-4}$	33.8	1.10	1.51	4.93	5
C <sub>12</sub> C <sub>3</sub> C <sub>14</sub> PB	$1.83 \times 10^{-4}$	$1.98 \times 10^{-4}$	34.6	1.27	1.31	4.56	6
C <sub>10</sub> C <sub>3</sub> C <sub>14</sub> PB	$2.23 \times 10^{-4}$	$2.3 \times 10^{-4}$	35.0	1.50	1.11	4.34	8
C <sub>8</sub> C <sub>3</sub> C <sub>16</sub> PB	$3.06 \times 10^{-5}$	$3.6 \times 10^{-5}$	33.1	1.77	0.94	5.15	2

<sup>a</sup>  $N^*$  represents the micellar aggregation number  $N_{agg}$  at *cmc*.

**Table 2.** Thermodynamic parameters of micellization at different temperatures.

Surfactants	T (°C)	<i>cmc</i>	$\alpha$	$\beta$	$\Delta G_m^0$	$\Delta H_m^0$	$-T \cdot \Delta S_m^0$
		mmol/L			kJ/mol	kJ/mol	kJ/mol
C <sub>10</sub> C <sub>3</sub> C <sub>10</sub> PB	15	4.265	0.197	0.803	-29.57	-0.95	-28.62
	20	4.329	0.202	0.798	-29.92	-3.42	-26.50
	25	4.412	0.214	0.786	-30.09	-6.11	-23.98
	30	4.617	0.225	0.775	-30.18	-9.04	-21.14
	35	4.857	0.241	0.759	-30.13	-12.18	-17.95
C <sub>12</sub> C <sub>3</sub> C <sub>12</sub> PB	15	0.62	0.193	0.807	-35.70	-6.20	-29.50
	20	0.641	0.2	0.8	-36.02	-6.51	-29.51
	25	0.668	0.221	0.779	-35.91	-7.65	-28.26
	30	0.697	0.223	0.777	-36.32	-9.87	-26.45
	35	0.74	0.245	0.755	-36.09	-12.96	-23.13
C <sub>14</sub> C <sub>3</sub> C <sub>14</sub> PB	15	0.102	0.23	0.77	-40.18	-7.02	-33.16
	20	0.107	0.258	0.742	-39.83	-9.65	-30.18
	25	0.114	0.272	0.728	-39.86	-13.13	-26.72
	30	0.124	0.28	0.72	-40.00	-17.53	-22.47
	35	0.138	0.286	0.714	-40.13	-22.89	-17.24
C <sub>12</sub> C <sub>3</sub> C <sub>14</sub> PB	15	0.182	0.296	0.704	-36.43	-3.11	-33.33
	20	0.19	0.313	0.687	-36.40	-7.80	-28.61
	25	0.198	0.324	0.676	-36.56	-11.48	-25.08
	30	0.217	0.33	0.67	-36.71	-14.11	-22.60
	35	0.234	0.341	0.659	-36.74	-15.48	-21.27
C <sub>10</sub> C <sub>3</sub> C <sub>14</sub> PB	15	0.202	0.642	0.358	-26.22	-6.81	-19.41
	20	0.211	0.645	0.355	-26.00	-7.37	-18.63
	25	0.23	0.663	0.337	-25.71	-7.70	-18.01
	30	0.238	0.679	0.321	-25.57	-7.81	-17.76
	35	0.256	0.683	0.317	-25.71	-7.78	-17.93
C <sub>8</sub> C <sub>3</sub> C <sub>16</sub> PB	15	0.027	0.796	0.204	-24.51	-7.08	-17.44
	20	0.03	0.805	0.195	-24.44	-12.61	-11.83
	25	0.036	0.809	0.191	-24.40	-14.90	-9.50
	30	0.041	0.811	0.189	-24.51	-13.65	-10.86
	35	0.047	0.809	0.191	-24.75	-8.53	-16.22

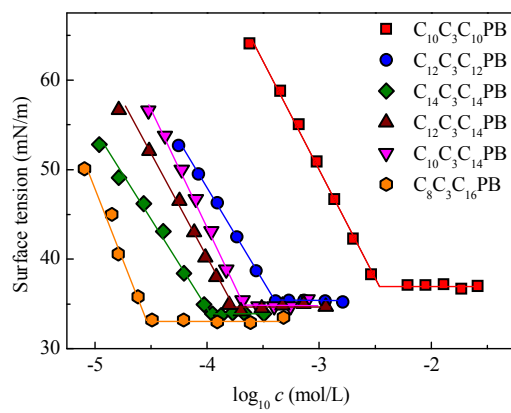


**Figure 1.**  $\gamma - \log_{10} c$  curves of Gemini surfactants in aqueous solutions at 25 °C.

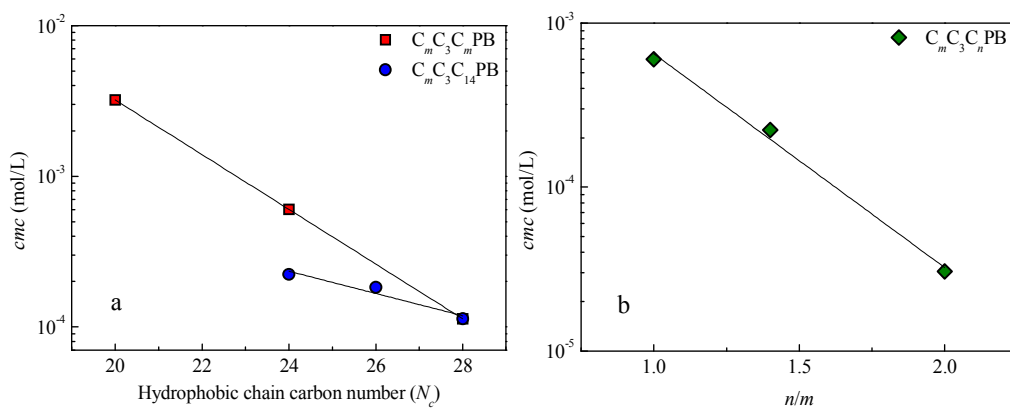


**Figure 2.** Effects of hydrophobic chain length (a) and dissymmetry (b) on *cmc*.

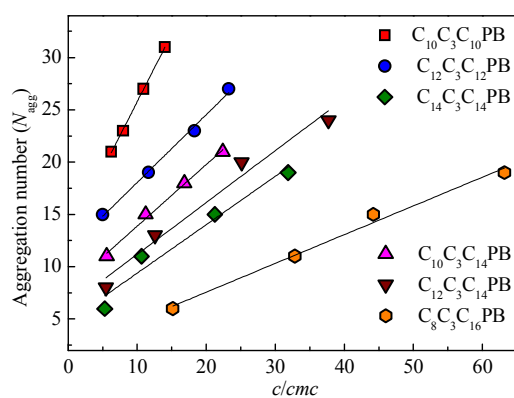


**Figure 3.** Concentration dependent micellar aggregation number ( $N_{agg}$ ) at 25 °C, the  $cmc$  values

adopted from surface tension measurements.

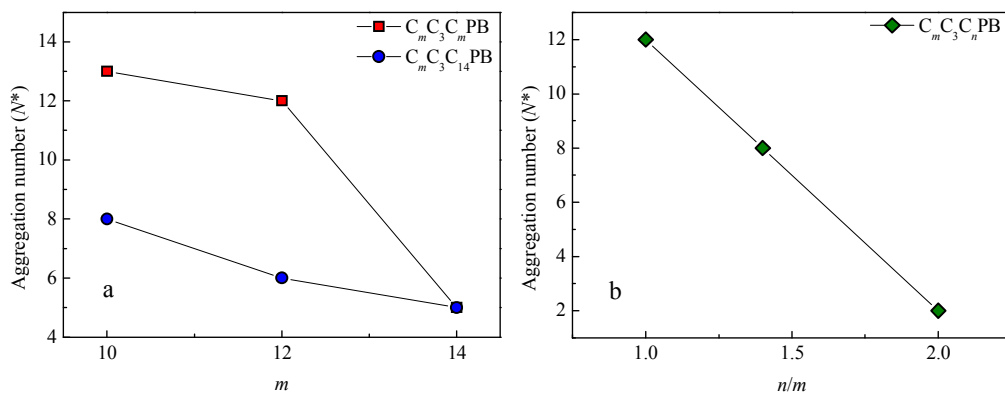


**Figure 4.** Effect of the hydrophobic chain length (a) and the dissymmetry (b) on  $N^*$  at 25 °C.

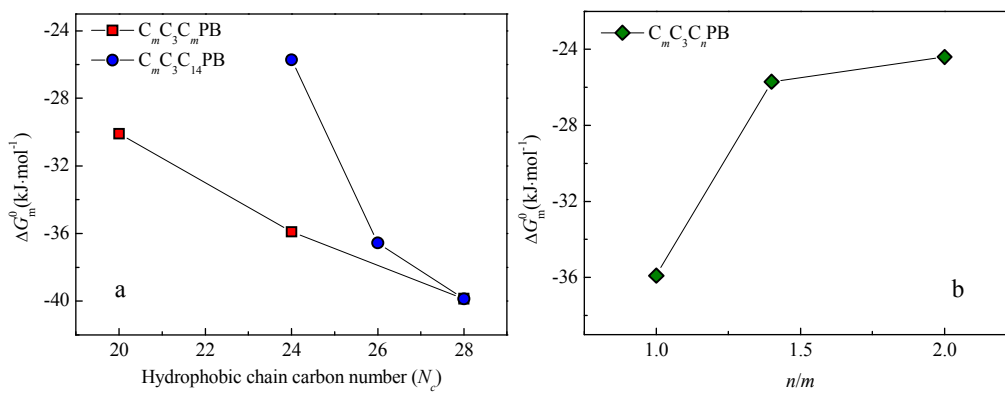


**Figure 5.** Effect of the hydrophobic chain length (a) and the dissymmetry (b) on  $\Delta G_m^0$  at 25 °C.

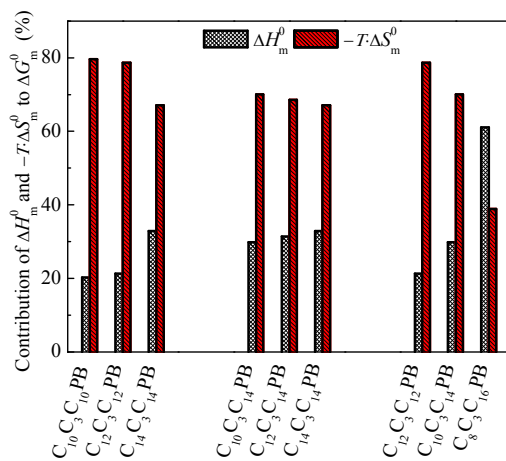


**Figure 6.** Contribution of enthalpy ( $\Delta H_m^0$ ) and entropy ( $-T \cdot \Delta S_m^0$ ) to Gibbs free energy ( $\Delta G_m^0$ ) at

25 °C.

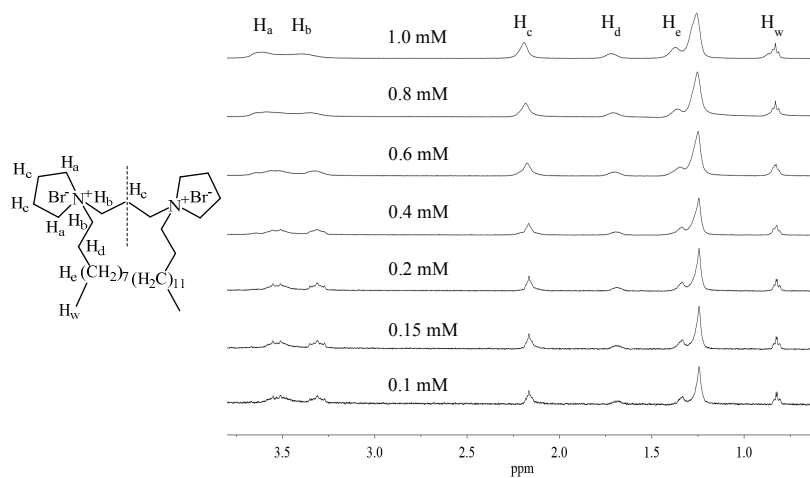


**Figure 7.** Concentration dependent  $^1\text{H}$  NMR spectra and proton numbering of  $\text{C}_{10}\text{C}_3\text{C}_{14}\text{PB}$  in  $\text{D}_2\text{O}$  at  $25\text{ }^\circ\text{C}$ .

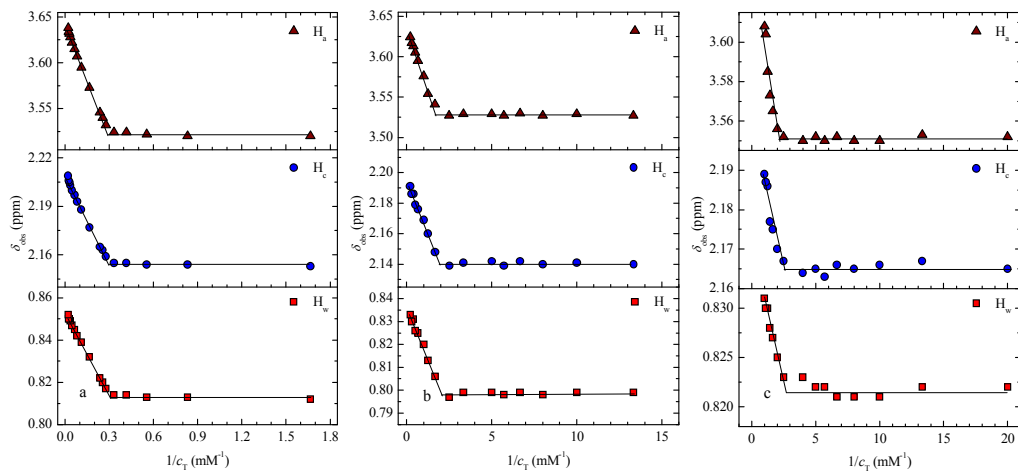


**Figure 8.** Plots of  $\delta_{\text{obs}}$  versus  $1/c_T$  for  $\text{C}_{10}\text{C}_3\text{C}_{10}\text{PB}$  (a),  $\text{C}_{12}\text{C}_3\text{C}_{12}\text{PB}$  (b) and  $\text{C}_{10}\text{C}_3\text{C}_{14}\text{PB}$  (c) at 25

$^{\circ}\text{C}$  in  $\text{D}_2\text{O}$ .

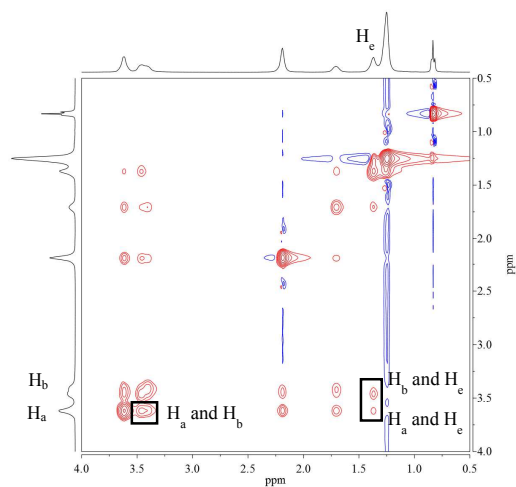


**Figure 9.** 2D Noesy NMR spectrum of 5 mM C<sub>12</sub>C<sub>3</sub>C<sub>12</sub>PB in D<sub>2</sub>O at 25 °C.